Aeolian sediment transport pathways and aerodynamics at troughs on Mars

Mary C. Bourke[1]
School of Geography and the Environment, University of Oxford, Oxford, United Kingdom

Joanna E. Bullard
Department of Geography, Loughborough University, Loughborough, United Kingdom

Olivier S. Barnouin-Jha
Applied Physics Laboratory, Johns Hopkins University, Laurel, Maryland, USA

Received 14 July 2003; revised 4 February 2004; accepted 2 April 2004; published 13 July 2004.

[1] Interaction between wind regimes and topography can give rise to complex suites of aeolian landforms. This paper considers aeolian sediment associated with troughs on Mars and identifies a wider range of deposit types than has previously been documented. These include wind streaks, falling dunes, "lateral" dunes, barchan dunes, linear dunes, transverse ridges, sand ramps, climbing dunes, sand streamers, and sand patches. The sediment incorporated into these deposits is supplied by wind streaks and ambient Planitia sources as well as originating within the trough itself, notably from the trough walls and floor. There is also transmission of sediment between dunes. The flow dynamics which account for the distribution of aeolian sediment have been modeled using two-dimensional computational fluid dynamics. The model predicts flow separation on the upwind side of the trough followed by reattachment and acceleration at the downwind margin. The inferred patterns of sediment transport compare well with the distribution of aeolian forms. Model data indicate an increase of wind velocity by ~30% at the downwind trough margin. This suggests that the threshold wind speed necessary for sand mobilization on Mars will be more frequently met in these inclined locations. *INDEX TERMS:* 1815 Hydrology: Erosion and sedimentation; 1824 Hydrology: Geomorphology (1625); *KEYWORDS:* Trough, aeolian, dune, MOC, MOLA, computational fluid dynamic modeling

Citation: Bourke, M. C., J. E. Bullard, and O. S. Barnouin-Jha (2004), Aeolian sediment transport pathways and aerodynamics at troughs on Mars, *J. Geophys. Res.*, *109*, E07005, doi:10.1029/2003JE002155.

1. Introduction

[2] A significant proportion of the surface of Mars is covered in aeolian deposits. Surface sediment frequently forms distinct morphological features such as mantles, wind streaks, dunes and a variety of sand sheet-like deposits [*Greeley and Iversen*, 1985; *Thomas et al.*, 1999]. Although wind-erodible sediment potentially exists over the whole planet, the major concentration of dunes is in vast sand seas of the northern hemisphere covering an area of 680,000 km^2 [*Lancaster and Greeley*, 1990]. Elsewhere, they occur in local concentrations often trapped by topographic features [*Greeley and Iversen*, 1985; *Malin et al.*, 1998]. It is important to understand the extent to which geological signatures of past fluvial activity on Mars have been modified. To date, there has been little focus on aeolian features associated with troughs and valleys on Mars, despite the potential for significant infilling and burial of fluvial features. Mars Orbital Camera (MOC) images show that there is an abundance of transverse bed forms on trough floors [*Malin and Edgett*, 2001] but other within-valley dune forms have not been identified. Valleys on Earth are known to act both as sediment sources in dune fields [*Lancaster*, 1986; *Mabbutt and Wooding*, 1983; *Wasson*, 1984] and as interceptors or "sinks" blocking or truncating sediment pathways. In previous studies, the approach to determine sediment sources, transport pathways and sinks has been global in scale [*Anderson et al.*, 1999]. Few studies have focused on the landform scale. There are some exceptions, notably work that has identified crater dune fields as sediment sources for wind streaks [*Edgett*, 2002; *Edgett and Malin*, 2000; *Thomas et al.*, 1981], the association of seif-like features with the elongation of barchan horns [*Lee and Thomas*, 1995; *Tsoar et al.*, 1979] and links between barchan and transverse dunes in Proctor crater [*Fenton et al.*, 2003].

[3] Topography affects both wind velocity and direction. Sediment transport and erosion may increase as wind veloc-

[1]Now at Planetary Science Institute, Tucson, Arizona, USA.

0148-0227/04/2003JE002155$09.00

ities increase on the windward side of topographic features such as hills and valleys [*Greeley et al.*, 2002] while zones of flow separation on the downwind side may be areas of preferential deposition [*Wiggs et al.*, 2002]. Wind flow patterns predicted by general circulation models for Mars and Earth generally correlate with the location and orientation of aeolian deposits [*Anderson et al.*, 1999; *Blumberg and Greeley*, 1996]. Research on the interactions between synoptic-scale wind flow and trough topography on Earth suggests that the presence of troughs will initiate not only a within-trough wind regime, but also may affect the strength and orientation of wind on the adjacent surface [*Bullard et al.*, 2000; *Sierputowski et al.*, 1995]. This, in turn, may affect the location of aeolian deposits [*Wiggs et al.*, 2002].

[4] We use the term trough to include all linear negative relief topography. The results reported here are valid for fluvial valleys, Chaos regions, Chasma etc., and are partly applicable to escarpments. However, the specific geological history will determine the sediment type and availability, which in turn will influence the potential assemblage of aeolian forms. Another influence will be the presence of niveo-aeolian deposits. In polar deserts on Earth, sand dunes may have permafrost cores and/or contain sand layers interbedded with snow and ice [*Calkin and Rutford*, 1974; *McKenna Neumann*, 2004; *Steidtmann*, 1973]. We are investigating the potential for niveo-aeolian dune deposits on Mars in ongoing research [e.g., *Bourke et al.*, 2004].

[5] This paper focuses on the interaction between trough topography and aeolian sediment on Mars. Using detailed observations from narrow and wide-angle MOC images of troughs in Syrtis Major (and elsewhere), the effects of the interaction between regional-scale wind patterns and trough topography on aeolian depositional forms are described. We highlight the range of dunes found within the trough, suggest potential sediment sources and consider the role of the trough as a temporary sediment sink and/or store. Using work that has been undertaken on valley-wind interaction on Earth [*Wiggs et al.*, 2002], a preliminary 2-D model is developed to investigate similar interactions under Martian conditions. We suggest that, through its impact on aeolian sediment transport pathways, the trough provides an important link (source/sink) for exchange of sediment between different aeolian forms and different parts of the surface. A conceptual model is presented illustrating the sediment transport continuum between the trough and the aeolian features both within and adjacent to it.

2. Study Area

[6] Syrtis Major is one of the most prominent Early Hesperian (~3.6 Gy) volcanic complexes on Mars. The gently sloping (~0.13°) lava plains are estimated to be between 0.5 and 1 km thick [*Hiesinger and Head*, 2004]. Syrtis Major is a low-albedo (0.15) and high thermal inertia (average 312.53 J m^{-2} K^{-1} $s^{-1/2}$) [*Fergason and Christensen*, 2002] region on Mars. Recent Thermal Emission Spectrometer (TES) data indicate the northern region of Syrtis Major to be predominantly basaltic [*Bandfield et al.*, 2000], specifically comprising feldspar and high calcium Pyroxene [*Mustard and Cooper*, 2002]. The principal surface types of the region include the following terrain components: old cratered, knobby, locally grooved, etched, pitted, polygonal terrain in craters, cratered and smooth terrain superimposed with dunes [*Hiesinger and Head*, 2004].

[7] At a regional scale, Syrtis Major is dominated by easterly winds. This is inferred from the orientation of wind streaks which are aligned between 260° and 280° (Figure 1). Arnus Vallis, located in northern Syrtis Major, is a sinuous, slot-like trough (Figures 1–3). It has a northeast-southwest orientation and crosses the east to west aeolian sediment transport path, as indicate by wind streak direction. Arnus Vallis is 200 km long and centered on 14.1°N 289.5°W sloping gently down to the north (Figure 4b). Other significant regional features include impact craters, troughs, wrinkle ridges, lava flow fronts and dark and bright wind streaks (Figure 1). The origin of the trough is unknown; however proximity to the Nili Patera caldera to the south suggests that it is likely to be a lava channel. A series of (sub) horizontal beds exposed in the trough wall may be lava deposits. The presence of an inner channel (Figure 3) suggests that Arnus Vallis may have been subject to low-viscosity fluid erosion, perhaps water released through geothermal activity.

3. Results

3.1. Trough Morphometry

[8] The MOC and MOLA data indicate that the trough has an average width of 775 m and a relative depth of ~90 m. The high-resolution MOC images show the trough to be sinuous, with well-developed convex and concave bends (Figure 3). The absence of craters on the trough floor indicates that it may be significantly younger than the surrounding Planitia surface on which a number of degraded craters are visible, although, craters may have been buried by trough floor aggradation. The MOLA profile indicates a sharp break of slope between the trough and Planitia surface that is sufficient to initiate flow separation at the upwind trough wall (Figure 4d).

3.2. Aeolian Deposits on the Planitia Surface

[9] We have based our observations primarily on a high-resolution (2.95 m/pixel) MOC image that reveals a 4.6 km length of Arnus Vallis in Syrtis Major (Figure 3). Two types of aeolian deposits are identified on the Planitia surface, wind streaks and drift deposits, and are described below.

3.2.1. Wind Streaks

[10] Wind streaks are identified by variations in albedo and take the form of dark, bright and mixed tone streaks that generally form in association with topographic obstacles such as troughs and craters [*Thomas et al.*, 1981]. In Figure 1, a series of bright and dark albedo markings extend from positive and negative topographic features (craters, ridges, and troughs). The east to west trend of these wind streaks (270°) correlates with global climate model predictions of regional wind directions [*Greeley et al.*, 1992]. Using the classification of *Thomas et al.* [1981], the streaks are identified as type I bright (b) and dark (d) wind streaks and are parallel and fan-shaped. Type I (d) streaks occur on the outer margins of approximately 30% of the bright streaks in Figure 1. High-albedo markings have been interpreted as global dust storm fallout deposits in protected wind-shadow zones [e.g., *Veverka et al.*, 1981]. Dark albedo

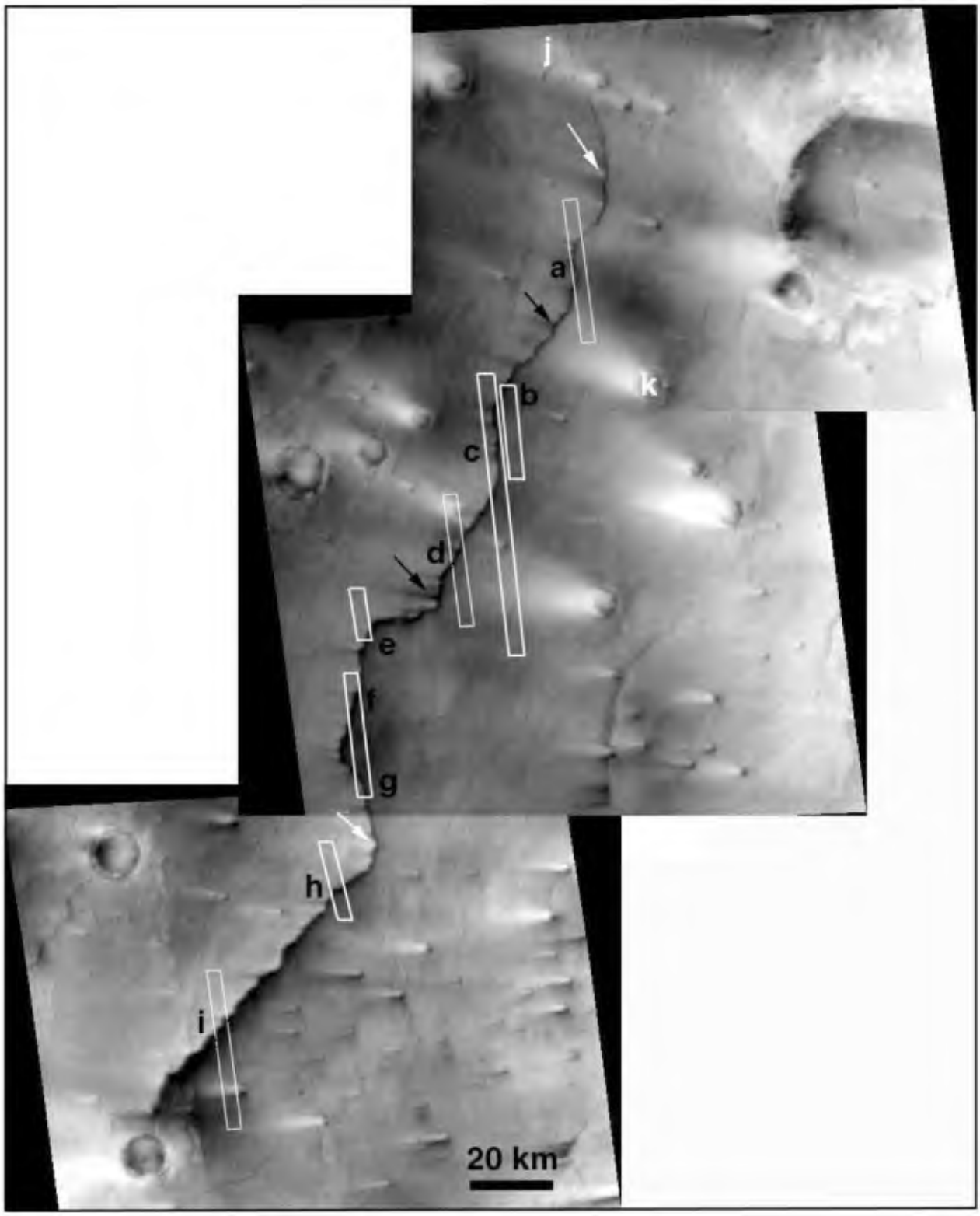

Figure 1. A mosaic of MOC wide-angle images: (bottom) E16-01895, 12.3°N, 290.12°W, 259.9 m/pixel, (middle) E16-00806, 14.17°N, 289.21°W, 261.13 m/pixel, and (top) E16-00279, 15.28°N, 288.75°W, 261.42 m/pixel. Arnus Vallis extends from the lower left. The location of MOC narrow-angle images (see Figure 2) is also shown. Arrows indicate examples where dark (black arrow) and bright (white arrow) streaks extend from trough; j: wind streak crosses trough; k: wind streak extending from crater does not appear to cross trough.

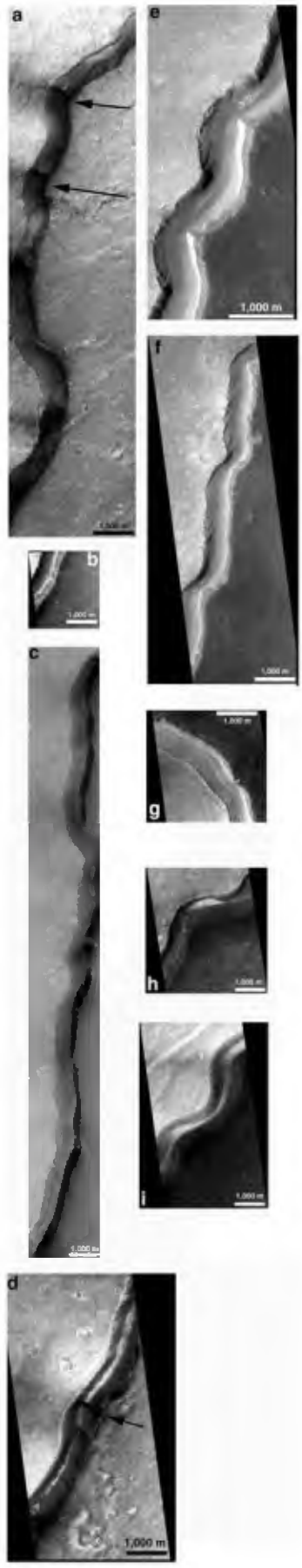

markings can form by the deposition or erosion of sediment [*Edgett*, 2002; *Thomas et al.*, 1981]. Both bright and dark albedo markings feed into and extend from Arnus Vallis (Figures 1 and 2). On the downwind side the bright streaks are similar to the coalesced individual bright streaks reported by *Thomas et al.* [1981]. The dark areas extending from the trough are assumed to be coalesced dark wind streaks. Dark streaks emanating from troughs have not previously been reported. We suggest that the classification of *Thomas et al.* [1981] be expanded to include these dark albedo features (Type II (d)). Most of the bright and dark albedo markings are discontinuous across the trough (Figure 1) suggesting a change in streak composition. The details of the relatively high-albedo markings are seen on the MOC image (e.g., Figure 3) and are identified as drift deposits. Some low-albedo areas are also depositional (see Figure 2a).

3.2.2. Drift Deposits

[11] Drift deposits are accumulations of wind blown particles not organized into bed forms [*Greeley et al.*, 2002]. The relatively high-albedo area on the downwind side of Arnus Vallis (Figure 3) appears to be a thin, discontinuous, sediment sheet and the dark albedo area upwind appears devoid of (relatively high-albedo) sediment at this resolution. The intensity of brightness on the downwind trough margin varies (Figure 3), and areas with higher albedo are inferred to be concentrations of aeolian sediment. We infer two types: sand patches and sand streamers (Figure 3). Sand patches are irregularly shaped areas, the largest measuring 1.7 km^2. Some appear to be trapped in topographic lows such as degraded impact craters (Figure 3). Sand streamers are narrow, slightly sinuous and sometimes discontinuous. They have an average width of 12 m and are of variable length (100–400 m). The two types of deposit appear to be linked and streamers frequently feed into and extend from patches. *Lancaster* [1996] suggests that sand patches are initiated in a zone of spatially and temporally fluctuating winds and disperse as surface roughness increases and sand supply is reduced.

[12] We do not know the thickness of sand streamers on Mars but suggest that they are thin. On Earth, a 7 km long, 0.5 km wide streamer has a maximum depth of 2.5 m [*Schaber and Breed*, 1999], and smaller ones are known to

Figure 2. Subset of MOC narrow-angle images showing sections of Arnus Vallis (for location, see Figure 1). From north to south: (a) E16-00278, 15.31°N, 289.15°W, 4.67 m/pixel, (b) E22-01045, 14.69°N, 289.41°W, 6.2 m/pixel, (c) E11-00553, 14.37°N, 289.44°W, 6.21 m/pixel, (d) E16-00805, 14.9°N, 289.61°W, 4.66 m/pixel, (e) M03-07414, 13.97°N, 289.97°W, 2.94 m/pixel, (f) E23-01150, 13.5°N, 290.012°W, 4.65 m/pixel, (g) same as Figure 2f, (h) E18-01455, 12.98°N, 290.08°W, 6.2 m/pixel, and (i) E16-01845, 12.32°N, 290.51°W, 6.19 m/pixel. The lateral dune is visible on the east side of Arnus Vallis in all images. The dune is estimated to extend continuously >165 km. Small-scale (500–800 m wide) low-albedo streaks extend westward from the trough. Many are associated with cross-trough extensions of the lateral dune (dark arrows). This illustrates a cross-trough sediment transport pathway from the lateral dune to the dark depositional streaks.

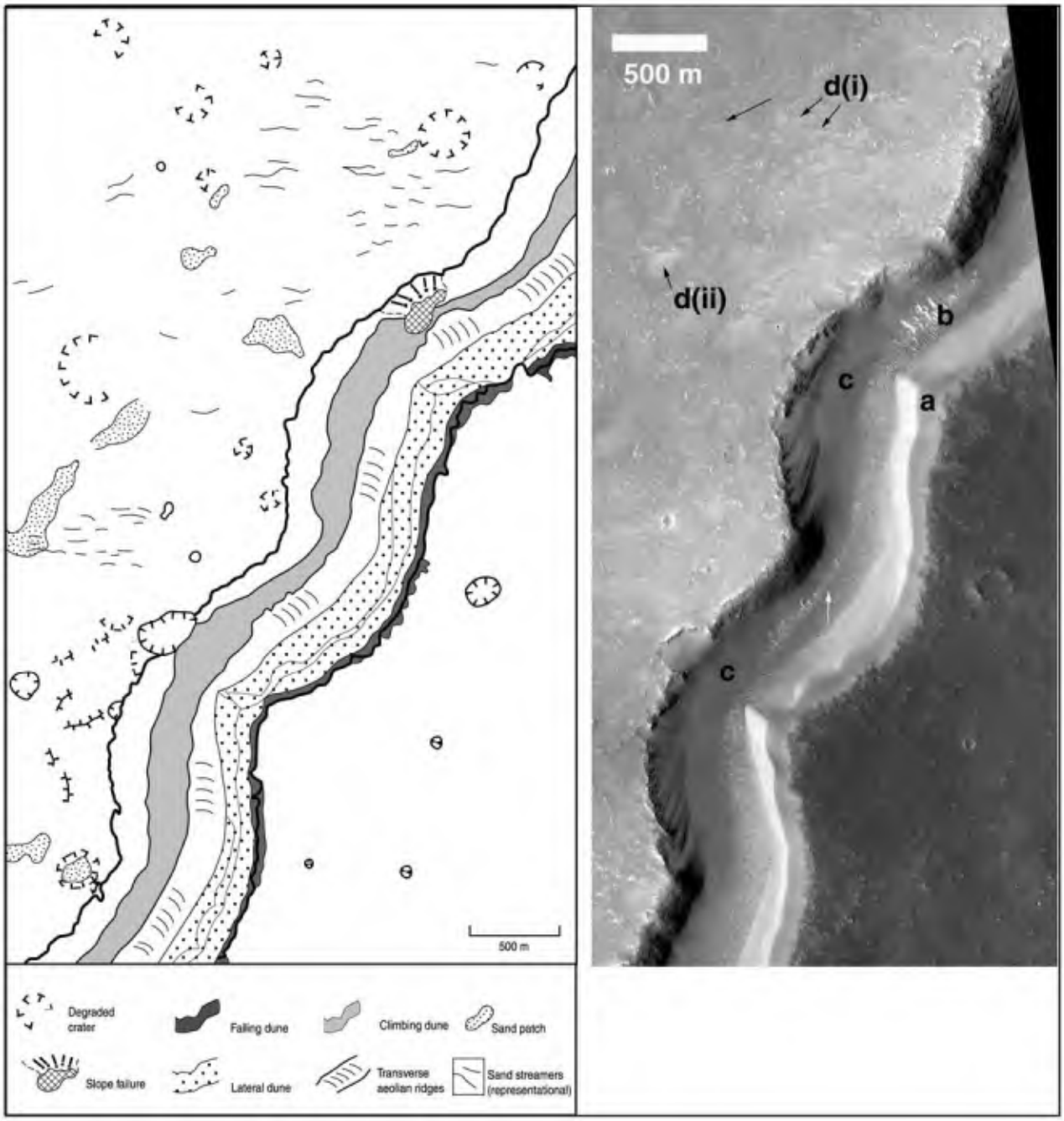

Figure 3. Geomorphic map of aeolian features and MOC image of Arnus Vallis (for location, see Figures 1 and 2e). (a) A large lateral dune extends along the eastern trough wall. (b) Transverse aeolian ridges are aligned along the trough floor, and (c) hypothesized sand ramps climb up the western trough wall. (d) Drift deposits: (i) sand streamers and (ii) sand patches. White arrow indicates western margin of an inner channel, the eastern boundary of which is buried by the lateral dune. Note the contrasting albedo on the east and west of the trough. MOC image (M03-07414), 13.97°N, 289.97°W, 2.95 m/pixel.

be significantly thinner. On Earth, sinuous sand streamers have been described as areas where throughflow dominates over accumulation and are consequently areas of the highest rates of transport [*Thomas*, 1997]. The albedo of these streamers and patches is similar to the distal portion of some bright wind streaks and similar sediment texture and processes may be found in those locations.

[13] *Greeley et al.* [2002] documented small-scale aeolian deposits at the Mars Pathfinder landing site (MPL). The features include small-scale (<5 m) dunes (whalebacks, transverse: barchan, barchanoid), normal ripples, megaripples and surface lag deposits. We do not have the resolution to determine the presence of these features at Arnus Vallis, but it is possible that the patches and streamers we identify

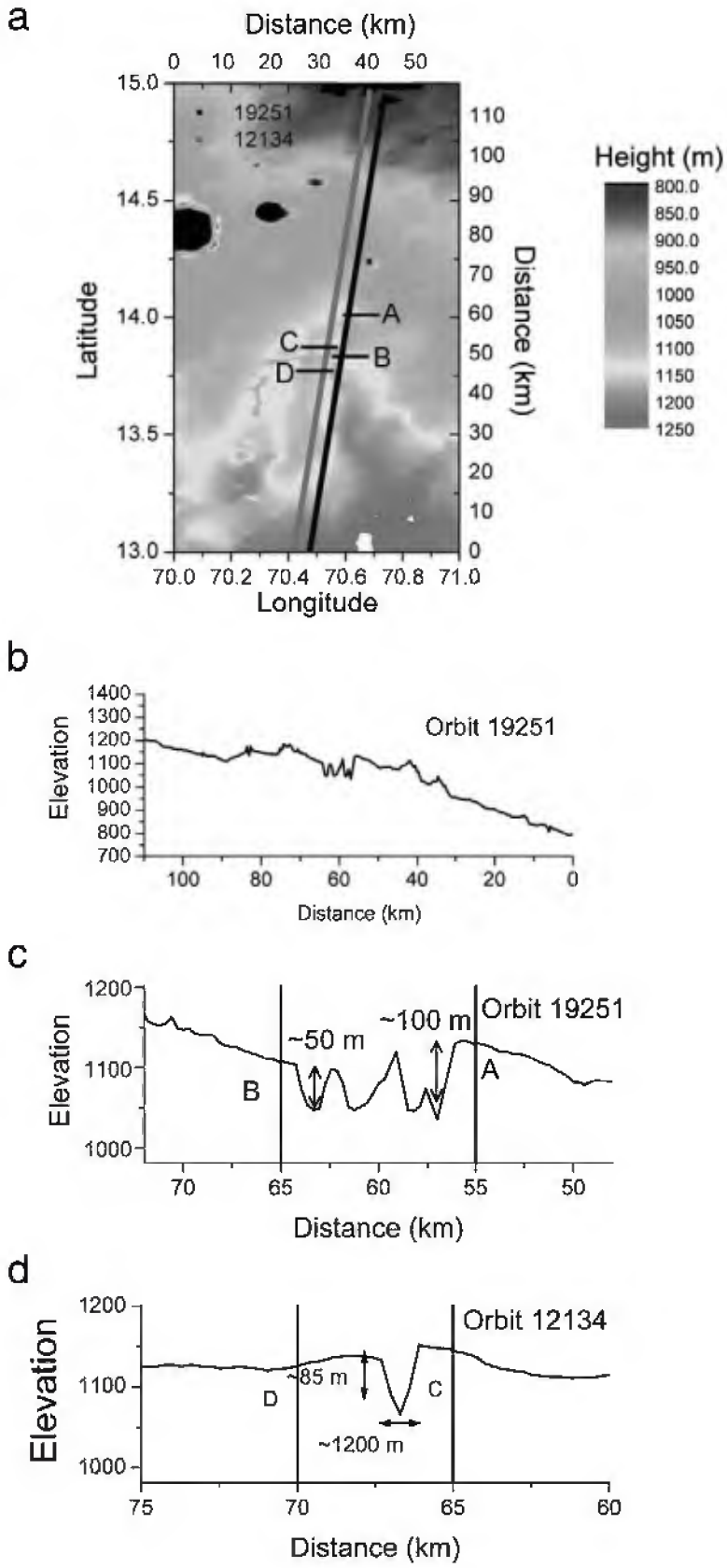
a
Distance (km)
0 10 20 30 40 50
15.0
14.5
14.0
13.5
13.0
Latitude
19251
12134
A
B
C
D
110
100
90
80
70
60
50
40
30
20
10
0
Distance (km)
Height (m)
800.0
850.0
900.0
950.0
1000
1050
1100
1150
1200
1250
70.0 70.2 70.4 70.6 70.8 71.0
Longitude
b
Elevation
1400
1300
1200
1100
1000
900
800
700
Orbit 19251
100 80 60 40 20 0
Distance (km)
c
Elevation
1200
1100
1000
~50 m
~100 m
Orbit 19251
B
A
70 65 60 55 50
Distance (km)
d
Elevation
1200
1100
1000
Orbit 12134
~85 m
D
C
~1200 m
75 70 65 60
Distance (km)

Figure 4

at 2.9 m/pixel resolution may alternatively be collections of lag surfaces and small-scale dunes and ripples similar to the MPL site.

3.3. Aeolian Deposits in Troughs

[14] The trough floor of Arnus Vallis is almost completely overlain by aeolian deposits. Four types of aeolian forms are identified. Falling dunes occur on the east of the trough at the junction with the Planitia surface; one third of the floor of the trough is occupied by a large "lateral" dune; transverse aeolian ridges occur in the base of the trough and sand ramps and dunes climb the downwind trough wall. Although not considered in detail in this paper, additional dune types noted in other troughs include linear, barchan, dome, network and star.

3.3.1. Falling Dunes

[15] Falling dunes are identified in Figure 3 as small-scale high-albedo areas between the trough edge and the lateral dune. Clearer examples are seen in Figure 11. They are between 50 and 75 m long, coalesce laterally and are the smallest of the aeolian dune features in the Arnus image. The relatively dark albedo of the surface adjacent to the falling dunes suggests that there is a high throughflow of sediment across the Planitia and all sediment is being deposited in the trough. However, some upwind locations along Arnus Vallis do have a high albedo (see Figures 2a and 2d), which indicates that deposition may occur on the Planitia surface upwind of the trough. We suggest that falling dunes concentrate significant sediment volumes into the trough and are important components in the sediment transport pathway. Falling dunes are not only associated with troughs as they have been reported in Proctor Crater [*Fenton et al.*, 2003] and observed on terrain with topographic obstacles (e.g., see MOC image FHA01366 from G. chaos). They are found on Earth on the downwind side of obstacles such as mountains [*Liu et al.*, 1999] and within valleys [*Li et al.*, 1999; *Seppala*, 1993].

3.3.2. Lateral Dune

[16] Within the trough, is a distinctive, topographically anchored dune that we term a lateral dune. The dune lies adjacent to the eastern trough wall and its alignment closely mirrors that of the trough. Planimetrically, it is very similar to valley-marginal dunes in southern Africa [*Bullard and Nash*, 2000] but in the Arnus example, the main body of sediment is contained within the trough rather than on the surrounding surface, as is found in the African examples. The falling dunes described above provide a sediment pathway linking the lateral dune to a sediment source on the Planitia surface to the east. The top of the dune averages 80 m wide and has a sinuous crest. The steep upper slope of the dune, grades into a lower-angle foot slope. The maximum width of the dune is ~285 m. The sharp crest and steep avalanche slopes indicate that this dune is being actively maintained. The position of the sinuous crest and steep avalanche face suggest that local vortices operating within the trough have sculpted the western face of the dune and suggest a secondary sedimentary transport path within the trough toward the north.

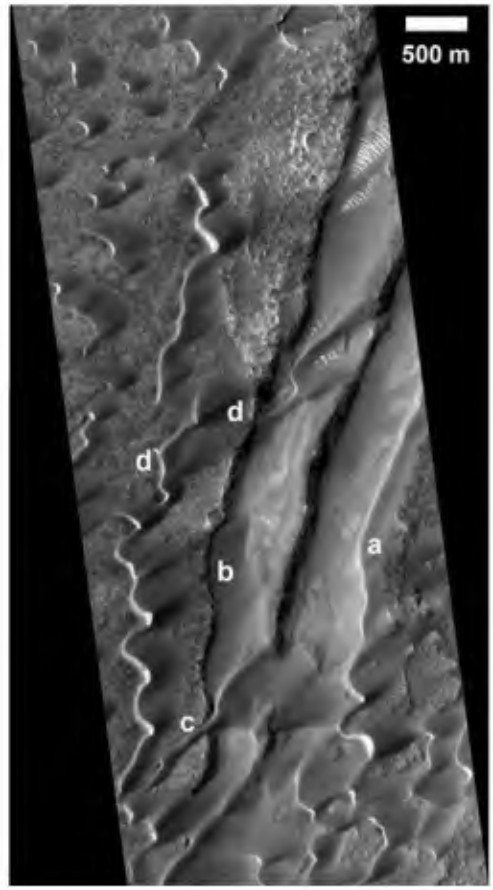

Figure 5. Trough and dunes in Nili Patera Caldera. MOC image M17-00435, 8.99°N, 293.29°W, 5.84 m/pixel. (a) Lateral dune. (b) Broad climbing dune. (c) Linear extension from a transverse dune. Linear dune (d) supplies sediment to barchanoid ridge (d') on the downwind surface.

[17] Two other examples of lateral dunes have been found, both located in Nili Patera Caldera (Figures 5 and 6). In the first example the dune is located at the upwind wall of two parallel troughs. Here the lateral dune is larger than that of Arnus Vallis and averages 195 m wide (W_{max} = 250 m; W_{min} = 170 m) despite a similar trough width (805 m). In the

Figure 4. MOLA data for Arnus Vallis site. The shot spacing is approximately 300 m, and each shot averages topography over a ~100 m ellipse. (a) MOLA topographic data calculated at 1/128 degrees in longitude and 1/256 in latitude resolution. Locations of MOLA transects 19251 and 12134 are shown. (b) Poleward plot of transect 19251 over 180 km length showing the general gentle dip to the north 0.0031 m/m. The transect generally parallels Arnus Vallis. (c) Detail of portion of transect 19251 at a zone where it intersects with the trough bottom. Data confirm a northward trending trough gradient and indicate that that portion of the trough has a gradient of approximately 0.0014 m/m, which is lower than the regional gradient. (d) Detail of portion of transect 12134, which traverses Arnus Vallis. The cross-trough profile illustrates that the windward side is approximately 25 m higher than the downwind trough side. Along the 1.25 km approach to the trough the gradient is 0.004 m/m. On the downwind side there is a convexity which may accelerate wind speeds and enhance particle transport.

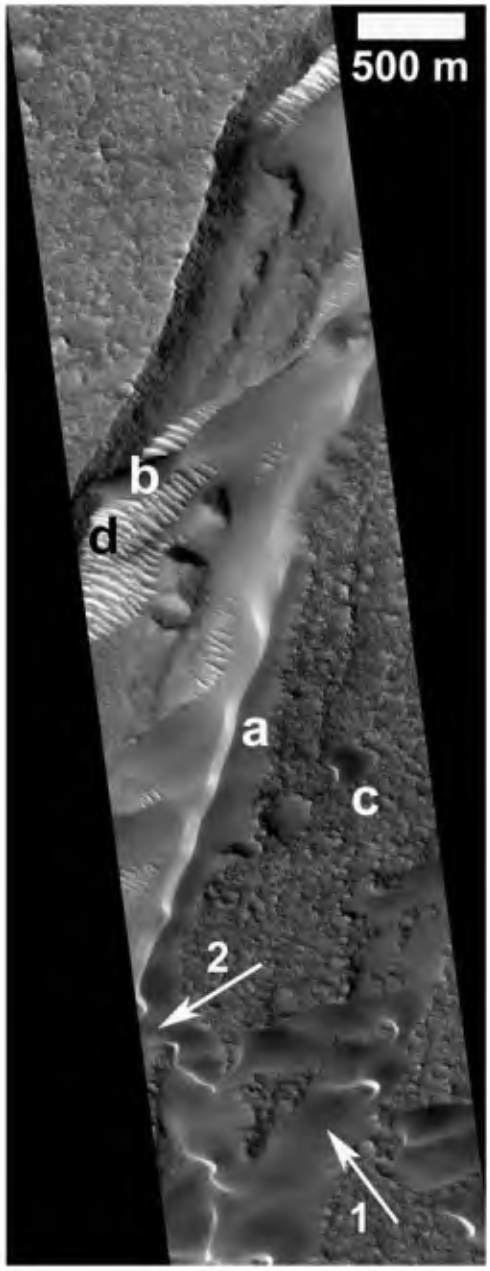

Figure 6. A 3 km section of a trough in Nili Patera caldera in Syrtis Major. A variety of dunes are present: (a) lateral, (b) linear, (c) barchan, and (d) transverse aeolian ridges (ripples/dunes). The 375 m wide trough has been heavily modified by aeolian sediment. Sand and barchan dunes fill shallow trough (arrow 1) and barchan limb crosses onto and merges with lateral dune in trough (arrow 2). MOC image (M10-01512), 9.27°N, 293.27°W, 2.92 m/pixel.

second example (Figure 6) the lateral dune averages 145 m wide (W_{max} = 185 m; W_{min} = 95 m), and stands approximately 15 m high in a trough 730 m wide and 100 m deep. In both of these examples the dune location and morphology is similar to that in Arnus Vallis.

3.3.3. Transverse Aeolian Ridges

[18] The floor of Arnus Vallis has a series of bed forms oriented perpendicular to the trough. These ridges are small features with wavelengths averaging 18 m (max. = 25 m, min. = 12 m). Ridge crest length averages approximately 140 m. These values fall within the distribution measured for similar features in narrow troughs (i.e., <600 m wide) on Mars [*Bourke et al.*, 2003]. Transverse forms (dunes and ridges) are the most common aeolian bed form on Mars [*Malin and Edgett*, 2001]. Their occurrence has been related to the relatively low volume of saltation load available and the unimodal transport regime [*Lee and Thomas*, 1995]. Transverse ridges are particularly abundant on valley floors [*Carr and Malin*, 2000], are aligned perpendicular to the valley direction, and are assumed to form transverse to the main wind direction [*Malin and Edgett*, 2001]. *Zimbelman and Wilson* [2002] measured the wavelength of similar but larger-scale transverse ridges in troughs ("ripple bands") on Syrtis Major (mean = 39 ± 16 m; crest length = 370 ± 236). On Earth the wavelength of dunes may be controlled by sediment supply and by grain size [*Wasson and Hyde*, 1983]. The smaller wavelength of the Arnus ridges compared with those in Syrtis Major may be related to a more abundant supply of sediment and/or finer grained sediment available on the trough floor [*Wilson*, 1972, 1973]. The crest length is controlled, for the most part by local trough floor topography, which in Arnus Vallis is primarily determined by the inner channel width.

3.3.4. Sand Ramps

[19] Low albedo deposits have accumulated along sections of the west trough wall of Arnus Vallis (Figure 3). They reach highest elevations in the north of the concave trough sections. The accelerated build-up in these wind-protected locations suggests a wind direction from the south. Their absence at convex reaches indicates a high shear zone along these trough sections with eddies/low velocity zones forming in the concave sections. The features have scalloped upper margins, and, in places, overlie the transverse ridges on the trough floor. MOLA profile data intersecting one such feature indicates it climbs to at least 25 m up the trough wall. The low-albedo sediment contrasts with the high albedo of the aeolian forms described previously. We infer a predominantly local source of sediment for these ramps in Arnus Vallis but do not exclude additional external sources. We interpret these deposits to be a series of sand ramps, where fine-grained slope debris from the trough wall (and possibly floor) is blown back up the trough wall. Sand ramps on Earth are commonly composed of mixed materials such as aeolian, fluvial and colluvial sediment [*Lancaster and Tchakerian*, 1996]. Sand ramps have not been previously reported on Mars.

3.3.5. Climbing Dunes

[20] In the Nili Patera troughs (Figures 5 and 6) dunes climb up the downwind trough wall. In Figure 5b the dune extends 1.35 km along the trough wall, appears steep, but does not climb over the lip of the trough at this resolution. Other examples of climbing dunes tend to be extensions of dune limbs that cross the trough floor (Figure 5). Climbing dunes have not been reported on Mars previously but are frequently observed on Earth associated with topographic obstacles along sediment transport pathways [*Howard*, 1985; *Lancaster and Tchakerian*, 1996]. They most commonly form on the upwind side of positive relief features such as a hill or escarpment when sand-transporting winds are obstructed, causing a loss of momentum and deposition.

The obstacle has to have a steep upwind slope (30–50 degrees) in order to effect dune forming conditions. If the slope is greater than 50 degrees, an echo dune, rather than a climbing dune, will form [*Cooke et al.*, 1993]. Where the sediment source is local, the size characteristics of particles at the base of the dune will be very similar to the source. Sediment size decreases with increased elevation up the dune as fine particles are winnowed from the source material and carried further up the dune slopes [*White and Tsoar*, 1998]. Climbing dunes are not only formed in association with positive relief but can also develop within valleys on the downwind valley slopes. Here, the valley floor or sediment entering the valley from the surrounding plateau, supplies sediment to form the dune. The sediment is transported across the valley and accumulates on the downwind valley slope gradually building up into a dune form. Within-valley climbing dunes on Earth are particularly associated with broad valleys but, with the exception of *Li et al.* [1999], few detailed studies of these features have been reported.

3.4. Simulated Flow Patterns on Mars

[21] Having described the aeolian features in the Arnus Vallis region of Syrtis Major, we can use their morphological and morphometric characteristics to consider, first, the relationship between regional- and local-scale wind flow patterns and, second, the interactions between the trough and the Planitia surface winds that determine aeolian sediment sources and transport pathways.

[22] As trough topography can have an impact upon regional surface winds, the following is a short review of recent wind tunnel and field studies of terrestrial conditions across a valley. *Wiggs et al.* [2002] have shown that in plateau landscapes with slot-channel relief the presence of the valley can initiate an acceleration of wind flow up to 1 valley width upwind due to a decreasing pressure gradient drawing air into the valley (Figure 7). Studies have also demonstrated a significant reduction in velocity as flow passes over the upwind edge of a valley or backward (downwind) facing escarpment [*Sierputowski et al.*, 1995; *Wiggs et al.*, 2002]. This is dependent upon the angle of approach of the regional wind compared with the valley orientation. Immediately downwind of the leading edge of the valley, any sediment being transported will be deposited. This is the mechanism which leads to the development of falling dunes and facilitates aeolian sediment accretion adjacent to the valley wall. In Figure 7b the point of flow reattachment is 0.7 of the valley width. Within the valley walls, wind speed is at a minimum in the center of the valley and flow accelerates toward the downwind valley edge often exceeding upwind velocities. A second zone of flow separation may develop on the plateau surface immediately downwind of the downwind valley edge [*Bowen and Lindley*, 1977; *Wiggs et al.*, 2002]. On the downwind plateau surface flow decelerates to recover toward velocities found upwind of the valley [*Wiggs et al.*, 2002] (Figure 7a).

3.4.1. Computational Fluid Dynamic Modeling

[23] In order to understand the spatial distribution of aeolian sediments at Arnus Vallis, we have undertaken preliminary 2-D computational fluid dynamic (CFD) modeling of the flow field generated in an isolated trough in a flat, plateau terrain under Martian conditions. As the MOLA

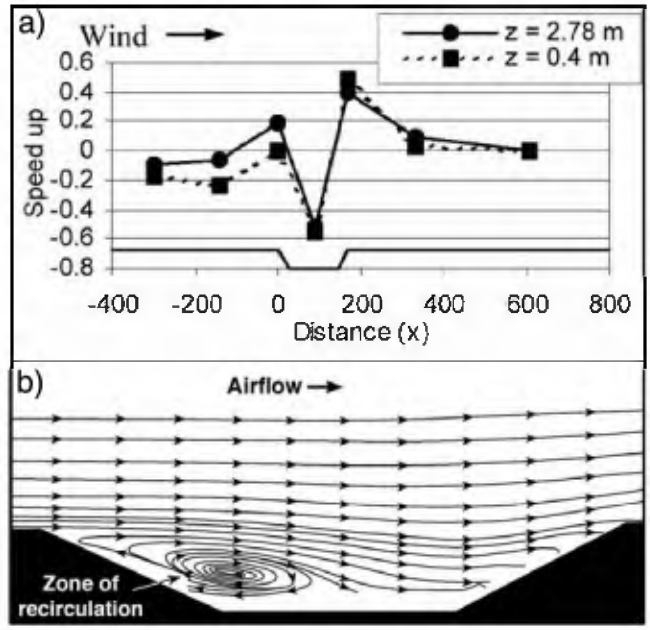

Figure 7. Experimental observations from wind tunnel [*Garvey et al.*, 2002] and field data [*Wiggs et al.*, 2002]. (a) Field data were collected on the Gaub River Namibia [*Wiggs et al.*, 2002]. The width:depth ratio for the Gaub River (7.9) is similar to Arnus Vallis (8.6). The graph shows the fractional speedup ratio [*Wiggs et al.*, 1996] measured at two heights (0.4 m and 2.8 m) above ground for a wind blowing normal to the valley axis. The valley position is shown at the bottom of the graph. (b) Cross-valley streamlines generated from wind tunnel data after *Garvey et al.* [2002]. Flow is from the left. Flow reattachment is at $x/l = 0.7$, $x/h = 5.6$.

spacing (300 m) and footprint (150 m) is too large to accurately represent Arnus Vallis in cross section, we consider a geometrically similar, but idealized situation where a wind blows steadily over the top of a canyon consisting of two 90 m vertical walls separated by an 800 m flat floor, and an 880 m plateau further downstream. This will permit us to gain a general overview of the flow structures generated by a valley under Mars atmospheric conditions. In addition, a valley with vertical walls represents a useful extreme where all possible wind eddies that may be generated in a trough can be seen. Changes in valley slopes are expected to alter eddy size and may in some instances even reduce their number.

[24] This preliminary model does not compute flow along a plateau upwind. Instead, we simply assume that wind entering the computational domain possesses a flat rather than a logarithmic velocity profile. A logarithmic profile is typically expected for a well-developed wind traveling along an upwind plateau. For Mars, the wind speed increases slowly ~100 m above the surface [*Greeley and Iversen*, 1985]. However, field and wind tunnel experiments [*Garvey et al.*, 2002; *Wiggs et al.*, 2002] indicate that the near surface winds accelerate as they pass over the upwind edge of a valley. In order to simulate this acceleration, we flatten the wind profile to better compute reasonable flow interactions within the trough. In addition, a test was run

Table 1. Martian Atmospheric Properties and Parameters Used in CFD Model

Martian Wind Properties	Value	Reynolds Number ($Re = uh\rho/\mu$)
Atmospheric density, ρ	0.02 kg/m^3	
Atmospheric viscosity, μ	2.238×10^{-5} Pa-s	
Upstream wall height, h	90 m	
Wind speed, u	1 m/s	0.8×10^5
	10 m/s	8.0×10^5
	20 m/s	16×10^5
Transition to turbulence		1.0×10^5–1.0×10^6

with a logarithmic wind profile. The change in the upwind re-circulation zone was found to be small, increasing it size by ~8%.

[25] The CFD used for this study was developed by *Ferziger and Pervic* [1996] and uses an implicit finite volume scheme with a pressure correction method (SIMPLE scheme). Table 1 lists typical Mars wind conditions, as well as atmospheric and flow parameters that are relevant to Arnus Vallis. Most notable is the Reynolds number (*Re*) that provides a measure of the inertial to viscous forces in a flow. When this number exceeds 10^5, inertial forces within a flow become important and generate random small-scale turbulence [*White*, 1986]. The scale of Arnus Vallis and the atmospheric conditions on Mars ensure that *Re* for flows within this trough are just within this turbulent regime (Table 1). In addition, surface roughness on the upstream plateau and within the Vallis probably ensures turbulent flow conditions. We thus use a version of the SIMPLE scheme that includes a κ-ε turbulent flow model, where κ parameterizes the turbulent energy of a flow and ε estimates the energy dissipation by turbulence in shear zones near surfaces and at the edge of obstacles. We use values of $\kappa = 0.015$ and $\varepsilon = 0.0037$ that are computed from the streamwise turbulence measured in the wind tunnel experiments of *Garvey et al.* [2002] using typical equations for estimating these parameters [*Barnouin-Jha et al.*, 1999].

[26] The boundary conditions used in our calculations are shown in Figure 8a. We assume that no slip occurs at the trough walls, floor or on the downstream plateau; that the upstream flow possesses a vertical flow profile; and that the top boundary permits slip parallel to its surface but no flow convection through the surface. This last condition in effect turns the top boundary into a symmetry plane, which we place far from the area of interest to ensure that no unrealistic accelerations occur in the flow due to area changes. *Barnouin-Jha et al.* [1999] have shown that placement of this boundary 800 m above the trough floor avoids such accelerations. Because we are considering steady state flows, the outflow conditions assume zero velocity gradients at the boundary and the same total mass flux as at the inlet.

[27] We performed calculations on three separate grids to determine which one would provide us with the most reasonable flow solution using the least amount of computational resources and time. The coarsest grid used had approximately 80 by 160 cells. The mesh was refined in the regions of interest, namely within the trough and near the downstream wall, but were kept coarse elsewhere. The intermediate and high-resolution grids were 4 and 16 times finer than this coarsest grid. The numerical method used in this study generates changes in the flow solution following each iteration. The computation was therefore run on all three grids employed until convergence where additional iterations caused no further change in the computed flow. The solutions obtained on the coarsest grid were significantly different from that seen on the other two finer grids. Very small changes, on the order of a few percent, were seen between the intermediate and highest resolution grids, although significant savings in computational time were obtained with the intermediate resolution grid. We therefore used the intermediate resolution grid to generate all the results presented in this study.

3.4.2. Model Results

[28] We present results for three wind speeds: 1m/s, 10m/s and 20m/s. The first two encompass the wind speeds measured by several of the Mars Landers on a typical Martian day [*Greeley and Iversen*, 1985; *Sullivan et al.*, 2000]. The last corresponds to typical wind speeds measured during Martian dust storms. Although the structures of turbulent flows are typically independent of flow speed, we present three flow speeds because *Re* for these flows are just greater than 10^5, the transition point between laminar and turbulent flow, and some *Re* dependence could be expected.

[29] Similar flow streamlines are produced for all three wind speeds (Figure 8). We see a zone of recirculation behind the upstream trough wall, recirculation associated with corner flow at the base of the downstream wall, acceleration of flow and flow separation at the top of the downstream trough wall, and formation of a subsequent recirculation zone on the downwind surface. All the flow patterns are consistent with the wind tunnel experiments presented by *Garvey et al.* [2002] except for the downstream corner flow re-circulation zone. This is because the wind tunnel experiments use shallow 20–25° inclined walls while our calculations possess steep 90° walls.

[30] The size of the recirculation zone generated near the upstream wall does not significantly vary with increasing flow speed (*Re*) and confirms that these flows are fully turbulent. Usually recirculation zones only vary for flow in the laminar regime, and under such conditions, depend primarily on *Re*. The location of the reattachment point is similar to that seen in the wind tunnel experiments [*Garvey et al.*, 2002] ($x/l = 0.7$), where l is valley width and x is horizontal distance ($x = 0$ at the leading edge of the valley). From our experiment we suggest that the extent of the recirculation region and the location of reattachment should be defined in terms of the height of the upstream wall as increasing the height of the valley would have more effect on the location of reattachment, than increasing valley width. If we redefine this reattachment point in terms of wall height, we then find that the wind tunnel experiments [*Garvey et al.*, 2002] occur at $5.6h$ where h is the upstream wall height. In our numerical results, this location is approximately at $5.9h$, which is essentially identical to that observed in the wind tunnel given that reattachments points determined from κ-ε models typically fall within 20% of those observed in wind tunnel experiments [*Nallasamy*, 1985].

[31] This modeled modification of the synoptic wind pattern by the trough has a number of implications for sediment transport adjacent to troughs on Mars. First,

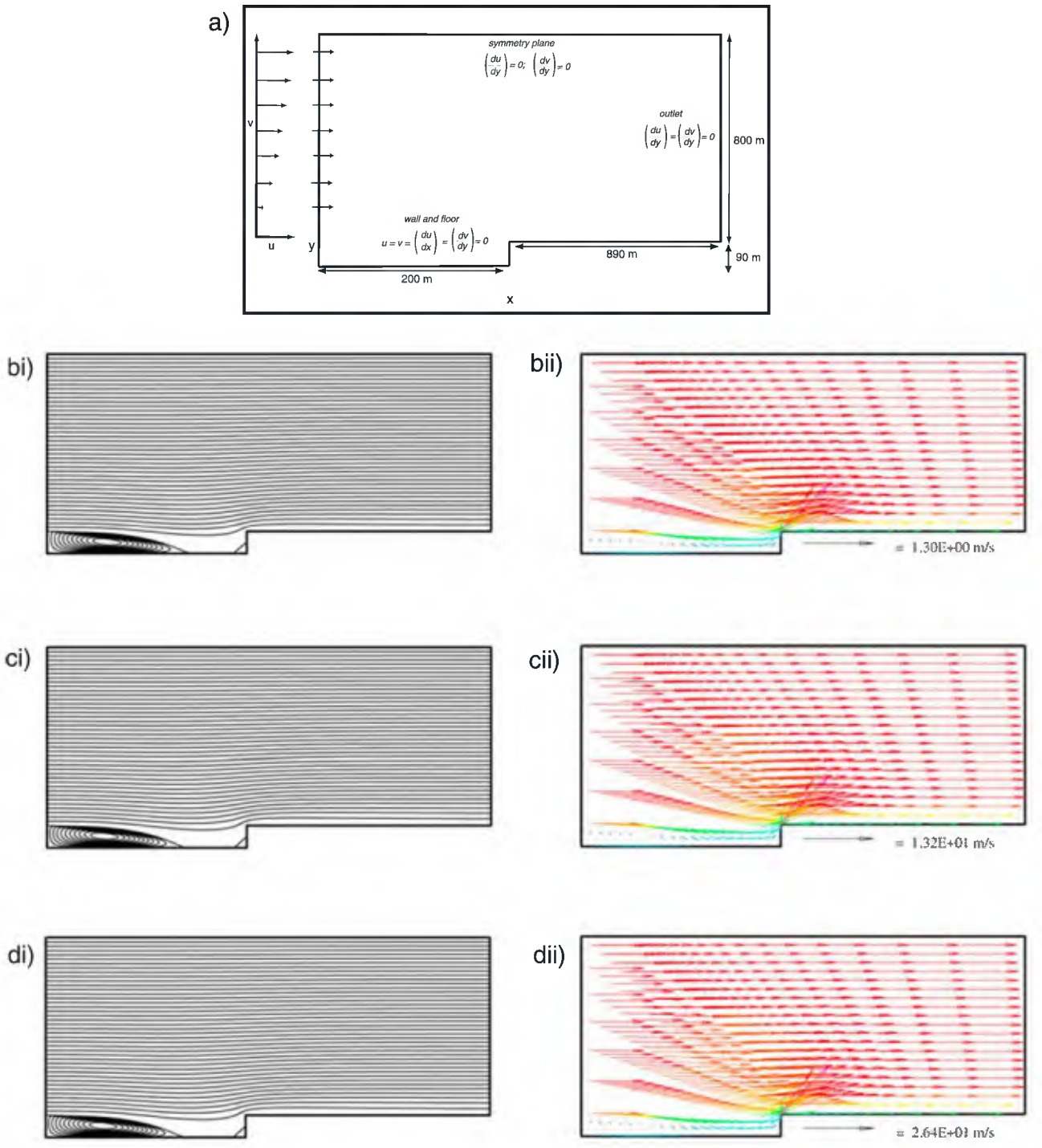

Figure 8. Results of CFD model: (a) the computational domain and the boundary conditions: u, horizontal velocity; v, vertical velocity. Streamline on left (bi, ci, di) and flow vector on right (bii, cii, dii); b is at 1 m/sec, c is at 10 m/sec, and d is at 20 m/sec. The red arrows are equal to the incoming flow speed. Reduced wind speeds are indicated in color from red, through yellow and green, and to blue. The arrow length indicates relative flow velocities. Modeled flow is from left to right. Flow reattachment is at $x/l = 0.7$, $x/h = 5.9$.

although we did not include the upwind plateau, the model of *Wiggs et al.* [2002] suggests that there will be a region immediately upwind of the trough where little or no aeolian deposition takes place due to accelerated flow. Figure 3 shows a dark zone on the upwind Planitia surface suggesting no sediment deposition has taken place, and/or erosion of the surface dust veneer by accelerated flow. Second, the CFD illustrates a zone of flow separation and consequent reduction in velocity at the upwind trough wall. We expect that, where sediment is available, significant amounts will

be deposited at the foot of the slope. Within Arnus Vallis, falling dunes and the lateral dune are located immediately downwind of the trough edge suggesting rapid flow deceleration. Third, there may be erosion or a zone of low/no deposition at the point of reattachment ($\sim 5.9h$). This zone is not clearly identifiable in the troughs examined and suggests wind flow along the valley axis is important. Fourth, there may be deposition in the recirculation zone at the foot of the downwind wall. Here we have found a series of climbing dunes and sand ramps. Sediment may be eroded from the sand ramps as flow accelerates at the trough wall. This may explain the process and identify the source of sediment to the sand streamers and patches downwind of the trough. This sediment movement will be more pronounced on walls less than 90°. Fifth, as the velocity increases at the top of the wall we suggest that sediment erosion/entrainment may be enhanced and would expect no or low deposition in this reach. Finally, beyond the trough we expect a zone of deposition. These findings support the conceptual model proposed by *Wiggs et al.* [2002].

[32] Although the model compares well with the distribution of sediment at many sites along Arnus Vallis, there are sites where, e.g., deposition is found on both the upwind and downwind trough margin. This variability is expected as there is dependence on local topography and sediment supply.

[33] The model indicates that maximum wind velocities are generated at the trough outlet. These velocities are an increase of 30%, 32% and 32% for 1, 10 and 20 m/sec upwind values. The topographically accelerated velocities are 1.3, 13.2 and 26.4 m/sec. Dunes on Mars have not actively migrated in the last ~30 years [*Edgett and Malin*, 2000; *Zimbelman*, 2000], but sand is active on dune crests [*Malin and Edgett*, 2001]. *Zimbelman* [2000] suggested that dune inactivity may be a factor of insufficient wind velocities. We have shown that topography can accelerate wind velocities under Martian conditions. It may be that current dune activity is limited to locations of accelerated flow and features such as sand streamers and climbing dunes associated with inclined topography should be targeted in future dune activity investigations.

3.5. Wind Direction

[34] Valley topography on Earth has been found not only to have an impact upon wind velocity, but also on wind direction [*Bullard et al.*, 2000; *Whiteman and Doran*, 1993]. *Bullard et al.* [2000] found, in experimental studies, that at any wind approach angle less than 90°, upstream regional winds are deflected to become more parallel to the valley orientation and this impact can extend up to 400 m upstream of the valley. *Wiggs et al.* [2002] found that wind deflection is more pronounced when the approach angle is <45°. When winds approach perpendicular to a valley there is no discernible change in direction, but wind velocities are affected. Arnus Vallis is oriented both broadly perpendicular to the regional wind regime and, in places, deviates away from it. We would expect some deflection of winds in these latter areas. Although bright and dark wind streaks are discontinuous across the trough, by examining streak orientation on either side we see that their orientation (270°) is not offset by the presence of the trough. Elsewhere on Mars, *Thomas et al.* [1981] reported that bright wind streaks that cross-trough complexes can be slightly offset but also show little or no deflection when they cross topography of 50 m or more.

3.6. Within-Trough Wind Regimes

[35] At the local scale, valleys on Earth can generate complex within-valley wind regimes as a result of processes such as thermal forcing, downward momentum transport and pressure-driven channeling. This can have an impact on aeolian bed form development in the trough with trough floor dunes usually forming perpendicular to the main trough strike as a result of unidirectional along trough winds. Most trough floor dunes and ripple-like features on Mars have a similar relative orientation suggesting that along-trough wind is the main determinant of the transverse ridge form. In Arnus Vallis, the transverse aeolian ridges have probably formed as a result of along-trough winds. The planimetric characteristics of the lateral dune, some of the larger transverse ridges and the sand ramps suggest that north-flowing winds have recently had a greater influence on landform development than south-flowing winds (Figure 3).

3.7. Aeolian Sediment Source

[36] Four potential sediment sources for aeolian deposits in troughs have been identified; wind streaks, ambient Planitia sediment, dunes and the trough (walls and floor). In addition, intradune nourishing is proposed as an important component in the sediment transport pathway. The following section is represented in Figure 9.

3.7.1. Supply to the Trough

3.7.1.1. Wind Streaks

[37] Type I b wind streaks feed sediment into the upwind side of Arnus Vallis but are discontinued on the downwind trough margin. This indicates that Arnus Vallis interrupts the sediment transport continuum across Syrtis Major. One of the controls on streak discontinuity may be proximity to the streak source. In a location to the north along Arnus Vallis, a bright streak extends continuously across the trough (Figure 10). The streak is initiated at a crater 3.5 km from the trough. The continuity of the streak and the absence of shadow in the trough suggest that sediment from the wind streak has infilled the trough. It is also possible that the deposit is dust fallout. As there are no MOC data for this location, Figure 11, from Candor Chasma, indicates a potential mechanism for sediment transport across a trough. Low-albedo sand enters the trough as falling dunes (Figure 11a). Linear forms cross the trough and climb the downwind wall facilitating a sediment transport continuum across the trough. The Arnus Vallis example illustrates the potential importance of wind streaks as a source of within-trough sediment. Others have found that in addition to dust, streaks may contain fine sand [e.g., *Edgett*, 2002; *Pelkey et al.*, 2001; *Thomas et al.*, 1981; *Zimbelman*, 1986]. *Pelkey et al.* [2001] were unable to determine the grain size of wind streaks south of Arnus Vallis within the limitations of the available data. This study suggests that some wind streaks in Syrtis Major may contain a fine sand fraction which, upon reaching the trough is stored in a range of aeolian bed forms. Troughs are not necessarily endpoints of the transport pathway as shown by dark streaks that extend downwind from a trough in Candor

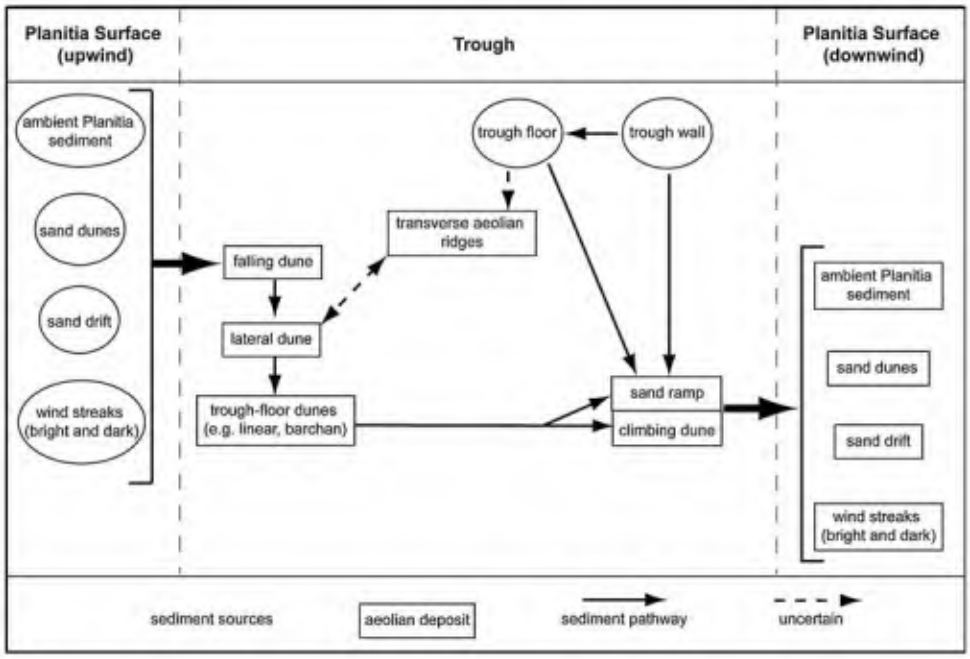

Figure 9. Conceptual model of sediment transport pathways associated with trough and valley features on Mars.

Chasma (Figure 11). The barchan dunes indicate that these dark albedo streaks are composed of sand. This suggests that, despite acting as a sediment store, troughs do not trap the sand fraction but permit throughflow through the construction of sand ramps, climbing dunes and at topographic low points (see also Figures 5 and 6).

3.7.1.2. Ambient Planitia Sediment

[38] Some relatively high-albedo areas upwind of Arnus (Figures 2a and 2d) are not obviously associated with wind streaks and may be examples of ambient sediment supply to the trough. The sediment appears to be arranged into sand streamers and patches similar to those described above. Any link to wind streaks is as yet unproven, but they may be a mechanism of sediment transport across the surface of Mars that is particularly active in locations where velocities are topographically accelerated.

3.7.1.3. Dunes

[39] In Nili Patera Caldera, barchan dunes are observed upwind and downwind of the troughs. In Figure 6 the elongated arm of a barchan dune is seen to extend over the trough wall and onto the surface of the lateral dune. This is clear evidence that a principal source of sediment for the lateral dune is from outside the confines of the valley, specifically, dunes on the upwind surface.

3.7.2. Within-Trough Sources

[40] The trough walls contribute sediment to the trough by slope failure (Figure 3), and probably aeolian abrasion and granular disintegration. Slope sediment has been

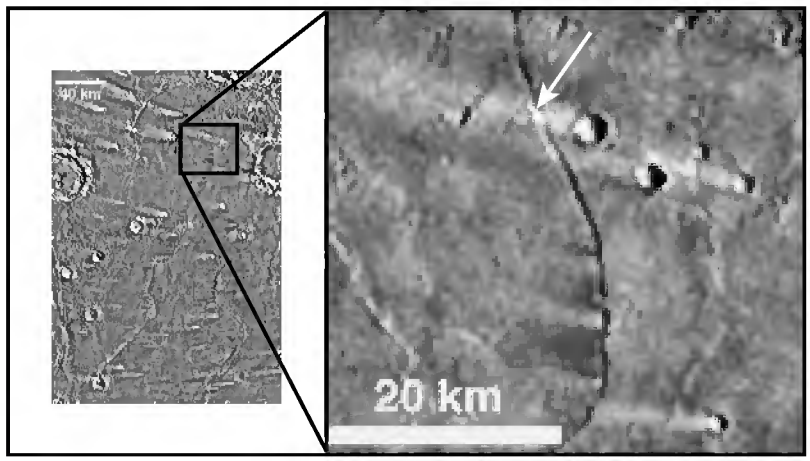

Figure 10. Viking image (S52188, 341 m/pixel) showing principal surface features in the region of Arnus Vallis (image center). Location of enlarged subset is shown by box. Subset indicates the location of the hypothesized trough filling (arrow) by sediment from a wind streak.

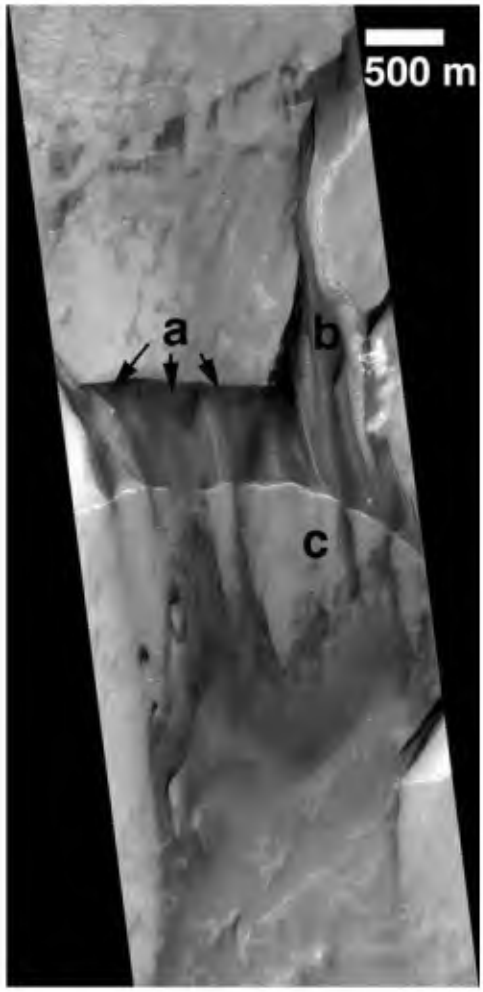

Figure 11. Trough in central Candor Chasma, MOC image E03-00746, 7.01°S, 72.69°W, 4.30 m/pixel. Image shows significant infilling of trough with sand: (a) low-albedo falling dunes, (b) linear dune, and (c) low-albedo linear and barchan dunes on downwind side of trough.

remobilized into sand ramps and climbing dunes. It is likely that the trough floor is a source of sediment for aeolian dunes, particularly the transverse aeolian ridges. However, as yet, this can only be inferred as no data currently exist to confirm the hypothesis. Others have also interpreted a local sediment source for bright transverse forms [*Fenton et al.*, 2003; *Malin et al.*, 1998].

[41] Within troughs, dunes may supply sediment to other dune forms. The MOC image from Candor Chasma (Figure 11) illustrates the movement of sediment across a 700 m wide trough. In the upper part of the figure a series of falling dunes (one 314 m long), supplies sediment to linear dunes that extend across the trough floor. These then form climbing dunes and feed dark streaks on the downwind side of the trough. A similar relationship is seen in the Nili Patera (Figures 5 and 6).

3.7.3. Trough as a Source for Planitia Sediment

[42] The absence of dark albedo sediment on the western Planitia surface in Figure 3 suggests that the low-albedo sediment in sand ramps and climbing dunes may not extend over the trough wall in all reaches of Arnus Vallis (although see Figures 2a and 2d). MOC images of troughs in Candor Chasma and Nili Patera suggest that the supply of sediment from the trough to the adjacent surface downwind is not dependent on a continuous climbing dune form over the lip of the trough. In Figure 5 a linear extension from a dune on the trough floor extends up the trough wall. Although the dune does not overtop the trough edge, there is an alignment of sediment trailing directly from the climbing dune toward a barchan form on the downwind surface (d-d′). A second example is seen in Figure 5c where the linear limb of a barchan form on the trough floor extends across a breach in the trough wall to feed into a small barchan.

3.7.4. Summary of Sediment Sources and Pathways

[43] Several sediment sources for aeolian deposits in troughs have been identified. A trough can act as both a throughflow area for aeolian sediment as well as a store, sometimes being significantly modified by the aeolian deposits. Wind streaks and ambient Planitia sediments, and in certain locations dunes, are sediment sources and means by which sediment is transported across a surface on Mars. Troughs (and valleys) will act as topographic barriers to sediment flux, temporally storing sediment in a range of bed forms. Under appropriate conditions and nourished by sources within the trough, sediment is supplied to the downwind Planitia surface. These data show that different styles of aeolian deposit can be both physically connected and linked as sinks and sources along sediment transport pathways. Geomorphic signatures of fluvial processes along these pathways can be significantly modified.

4. Estimating Sediment Storage

[44] Syrtis Major has been identified as a significant depocenter for global-scale aeolian sediment fluxes [*Anderson et al.*, 1999]. In addition, it is an area that has been subjected to major aeolian deflation [*Hiesinger and Head*, 2004] and so is presumably itself a significant source of sediment. Therefore understanding sediment fluxes across the region is important. We have identified that sediment moving across the Planitia is trapped in Arnus Vallis. The large linear dune is present in all available MOC images for the trough (Figures 2a–2i). Using the MOC and MOLA data sets and assuming that the lateral dune extends for the full length of the trough, we have calculated that the lateral dune in Arnus Vallis stores approximately 1.4 billion m^3 of aeolian sand at present.

5. Conclusion

[45] Valleys and troughs on Mars may be important storage areas for aeolian deposits. This paper has described a wider range of aeolian deposits associated with valleys and troughs than has previously been documented. These include: wind streaks, falling dunes, lateral dunes, barchan dunes, linear dunes, transverse ridges, sand ramps, climbing dunes sand streamers and sand patches.

[46] The source of sediment for aeolian deposits in troughs and the potential importance of a regional-scale input have not been previously considered. The aeolian sediment transport system across Syrtis Major (as indicated by the example of Arnus Vallis) illustrates the complex and dynamic nature of linked sediment storages that can exist on

Mars. Assemblages of deposits are often physically linked and form an active sediment transport continuum.

[47] The range of aeolian deposits recorded at Arnus Vallis (and in the Nili Patera Caldera and Candor Chasma) may be inherently linked to regions of high sediment flux, wind streak development and the presence of troughs and valleys.

[48] Computational fluid dynamic modeling of flow across a trough indicates a zone of flow separation at the foot of the upwind trough wall, reattachment at $5.9h$ and accelerated flow at the downwind valley wall. These model results match the pattern and distribution of aeolian forms associated with Arnus Vallis.

[49] **Acknowledgments.** This research was funded by NASA MDAP grant NAG5-11090. The authors acknowledge the use of Mars Orbiter Camera images processed by Malin Space Science Systems that are available at http://www.msss.com/moc_gallery/. We thank Peter Thomas and Giles Wiggs for helpful reviews. M.B. wishes to thank Rebecca Williams (Malin Space Science Systems), who targeted Arnus Vallis for more complete MOC coverage.

References

Anderson, F. S., R. Greeley, P. Xu, E. Lo, D. G. Blumberg, R. M. Haberle, and J. R. Murphy (1999), Assessing the Martian surface distribution of aeolian sand using a Mars general circulation model, *J. Geophys. Res.*, *104*(E8), 18,991–19,002.

Bandfield, J. L., V. E. Hamilton, and P. R. Christensen (2000), A global view of Martian surface compositions from MGS-TES, *Science*, *287*, 1626–1630.

Bamouin-Jha, O. S., P. H. Schultz, and J. Lever (1999), Investigating the interactions between an atmosphere and an ejecta curtain: 2. Numerical experiments, *J. Geophys. Res.*, *104*, 27,117–27,132.

Blumberg, D. G., and R. Greeley (1996), General circulation models, *J. Climatol.*, *9*, 3248–3259.

Bourke, M. C., S. A. Wilson, and J. R. Zimbelman (2003), The variability of transverse aeolian ridges in troughs on Mars, *Lunar Planet. Sci., XXXIV*, abstract 2090.

Bourke, M. C., M. Balme, and J. R. Zimbelman (2004), A comparative analysis of barchan dunes in the intra-crater dune fields and the North Polar Sand Sea, *Lunar Planet. Sci., XXXV*, abstract 1453.

Bowen, A. J., and D. Lindley (1977), A wind-tunnel investigation of the wind speed and turbulence characteristics close to the ground over various escarpment shapes, *Boundary Layer Meteorol.*, *12*, 259–271.

Bullard, J. E., and D. J. Nash (2000), Valley-marginal sand dunes in the south-west Kalahari: Their nature, classification and possible origins, *J. Arid Environ.*, *45*, 369–383.

Bullard, J. E., G. F. S. Wiggs, and D. J. Nash (2000), Experimental study of wind directional variability in the vicinity of a model valley, *Geomorphology*, *35*, 127–143.

Calkin, P. E., and R. H. Rutford (1974), The sand dunes of Victoria Valley, Antarctica, *Geogr. Rev.*, *64*(2), 189–216.

Carr, M. H., and M. C. Malin (2000), Meter-scale characteristics of Martian channels and valleys, *Icarus*, *146*(2), 366–386.

Cooke, R. U., A. Warren, and A. S. Goudie (1993), *Desert Geomorphology*, UCL, London.

Edgett, K. S. (2002), Low-albedo surfaces and eolian sediment: Mars Orbiter Camera views of western Arabia Terra craters and wind streaks, *J. Geophys. Res.*, *107*(E6), 5038, doi:10.1029/2001JE001587.

Edgett, K. S., and M. C. Malin (2000), New views of Mars eolian activity, materials, and surface properties: Three vignettes from the Mars Global Surveyor Mars Orbiter Camera, *J. Geophys. Res.*, *105*(E1), 1623–1650.

Fenton, L. K., J. L. Bandfield, and A. W. Ward (2003), Aeolian processes in Proctor Crater on Mars: Sedimentary history as analyzed from multiple data sets, *J. Geophys. Res.*, *108*(E12), 5129, doi:10.1029/2002JE002015.

Fergason, R. L., and P. R. Christensen (2002), Relationship between small scale surface features and thermal inertia units, *Lunar Planetary Sci., XXXIII*, abstract 1778.

Ferziger, J. H., and M. Pervic (1996), *Computational Methods for Fluid Dynamics*, 356 pp., Springer-Verlag, New York.

Garvey, B., G. F. S. Wiggs, I. P. Castro, and J. E. Bullard (2002), Wind tunnel and field investigation of flow dynamics within and around a valley, in *International Congress of Aeolian Research*, edited by J. Lee and T. M. Zobeck, pp. 29–34, Tex. Tech. Univ., Lubbock.

Greeley, R., and J. D. Iversen (1985), *Wind as a Geological Process on Earth, Mars, Venus and Titan*, 333 pp., Cambridge Univ. Press, New York.

Greeley, R., N. Lancaster, S. Lee, and P. Thomas (1992), Martian aeolian processes, sediments, and features, in *Mars*, edited by H. H. Kieffer et al., pp. 730–766, Univ. of Ariz. Press, Tucson.

Greeley, R., N. T. Bridges, R. O. Kuzmin, and J. E. Laity (2002), Terrestrial analogs to wind-related features at the Viking and Pathfinder landing sites on Mars, *J. Geophys. Res.*, *107*(E1), 5005, doi:10.1029/2000JE001481.

Hiesinger, H., and J. W. Head III (2004), The Syrtis Major volcanic province, Mars: Synthesis from Mars Global Surveyor data, *J. Geophys. Res.*, *109*, E01004, doi:10.1029/2003JE002143.

Howard, A. H. (1985), Interaction of sand transport with topography with local winds in the northern Peruvian coastal desert, in *International Workshop on the Physics of Blown Sand*, edited by O. E. Barndorff-Nielsen et al., pp. 511–544, Univ. of Aarhus, Aarhus, Denmark.

Lancaster, N. (1986), Grain size characteristics of linear dunes in the southwestern Kalahari, *J. Sediment. Petrol.*, *56*, 395–400.

Lancaster, N. (1996), Field studies of sand patch initiation processes on the northern margin of the Namib sand sea, *Earth Surf. Processes Landforms*, *21*(10), 947–954.

Lancaster, N., and R. Greeley (1990), Sediment volume in the North Polar sand seas of Mars, *J. Geophys. Res.*, *95*, 10,921–10,927.

Lancaster, N., and V. Tchakerian (1996), Geomorphology and sediments of sand ramps in the Mojave Desert, *Geomorphology*, *17*, 151–165.

Lee, P., and P. Thomas (1995), Longitudinal dunes on Mars: Relation to current wind regimes, *J. Geophys. Res.*, *100*(E3), 5381–5395.

Li, S., X. Liu, Y. Wang, H. Jin, Q. Wang, G. Dong, J. Shen, and P. Yang (1999), Formation mechanism and development pattern of aeolian sand landforms in Yarlung Zangbo River valley, *Sci. China, D42*, 272–284.

Liu, X. W., S. Li, and J. Y. Shen (1999), Wind tunnel simulation experiment of mountain dunes, *J. Arid Environ.*, *42*, 49–59.

Mabbutt, J. A., and R. A. Wooding (1983), Analysis of longitudinal dune patterns in the northwestern Simpson Desert, central Australia, *Z. Geomorphol. Suppl.*, *15*, 51–69.

Malin, M. C., and K. S. Edgett (2001), The Mars Global Surveyor Mars Orbiter Camera: Interplanetary cruise through primary mission, *J. Geophys. Res.*, *106*(E10), 23,429–23,570.

Malin, M. C., et al. (1998), Early views of the Martian surface from Mars Orbiter Camera on Mars Global Surveyor, *Science*, *279*, 1681–1685.

McKenna Neumann, C. (2004), Effects of temperature and humidity upon the transport of sedimentary particles by wind, *Sedimentology*, *51*(1), 1–17.

Mustard, J. F., and C. D. Cooper (2002), Comparison of ISM reflectance and TES emissivity measurements of Mars, *Lunar Planet. Sci., XXXIII*, abstract 1979.

Nallasamy, M. (1985), A critical evaluation of various turbulence models as applied to internal fluid flows, *NASA Tech. Pap. 2474*.

Pelkey, S. M., B. M. Jakosky, and M. T. Mellon (2001), Thermal inertia of crater-related wind streaks on Mars, *J. Geophys. Res.*, *106*(E10), 23,909–23,920.

Schaber, G. G., and C. S. Breed (1999), The importance of SAR wavelength in penetrating blow sand in northern Arizona, *Remote Sens. Environ.*, *69*, 87–104.

Seppala, M. (1993), Climbing and falling sand dunes in Finnish Lapland, in *The Dynamics and Environmental Context of Aeolian Sedimentary Systems*, edited by K. Pye, *Geol. Soc. Spec Publ.*, 72, 269–274.

Sierputowski, P., J. Ostrowski, and A. Cenedese (1995), Experimental study of wind flow over the model of a valley, *J. Wind Eng. Ind. Aerodyn.*, *57*, 127–136.

Steidtmann, J. R. (1973), Ice and snow in eolian sand dunes of southwestern Wyoming, *Science*, *179*(4075), 796–798.

Sullivan, R., R. Greeley, M. Kraft, G. Wilson, M. Golombek, K. Herkenhoff, J. Murphy, and P. Smith (2000), Results of the Imager for Mars Pathfinder windsock experiment, *J. Geophys. Res.*, *105*(E10), 24,547–24,562.

Thomas, D. S. G. (1997), *Arid Zone Geomorphology: Process, Form and Change in Drylands*, pp. 713, John Wiley, New York.

Thomas, P., J. Veverka, S. Lee, and A. Bloom (1981), Classification of wind streaks on Mars, *Icarus*, *45*, 124–153.

Thomas, P. C., et al. (1999), Bright dunes on Mars, *Nature*, *397*, 592–594.

Tsoar, H., R. Greeley, and A. R. Peterfreund (1979), Mars: The north polar sand sea and related wind patterns, *J. Geophys. Res.*, *84*, 8167–8180.

Veverka, J., P. Gierasch, and P. Thomas (1981), Wind streaks on Mars: Meteorological control of occurrence and mode of formation, *Icarus*, *45*, 154–166.

Wasson, R. J. (1984), Late Quaternary paleoenvironments in the desert dunefields of Australia, in *Late Cainozoic Paleoclimates of the Southern Hemisphere*, edited by J. C. Vogel, pp. 419–432, A. A Balkema, Brookfield, Vt.

Wasson, R. J., and R. Hyde (1983), Factors determining desert dune types, *Nature*, *304*, 337–339.

White, B. R., and H. Tsoar (1998), Slope effect on saltation over a climbing sand dune, *Geomorphology*, *22*, 159–180.
White, F. M. (1986), *Fluid Mechanics*, 732 pp., McGraw-Hill, New York.
Whiteman, C. D., and J. C. Doran (1993), The relationship between overlying synoptic-scale flows and winds within a valley, *J. Appl.*, 1669–1682.
Wiggs, G. F. S., I. Livingstone, and A. Warren (1996), The role of streamline curvature in sand dune dynamics: Evidence from field and wind tunnel measurements, *Geomorphology*, *17*(1–3), 29–46.
Wiggs, G. F. S., J. E. Bullard, B. Garvey, and I. Castro (2002), Interactions between airflow and valley topography with implications for aeolian sediment transport, *Physical Geogr.*, *21*(5), 366–380.
Wilson, I. G. (1972), Aeolian bedforms—Their development and origins, *Sedimentology*, *19*, 173–210.
Wilson, I. G. (1973), Ergs, *Sediment. Geol*, *10*, 77–106.
Zimbelman, J. R. (1986), Surface properties of the Pettit wind streak on Mars: Implications for sediment transport, *Icarus*, *66*, 83–93.
Zimbelman, J. R. (2000), Non-active dunes in the Acheron Fossae region of Mars between the Viking and Mars Global Surveyor eras, *Geophys. Res. Lett.*, *27*(7), 1069–1072.
Zimbelman, J. R., and S. Wilson (2002), Ripples and dunes in the Syrtis Major region of Mars, as revealed in MOC images, *Lunar Planet. Sci.*, *XXXIII*, abstract 1514.

O. S. Barnouin-Jha, Applied Physics Laboratory, Johns Hopkins University, Laurel, MD 20723, USA.
M. C. Bourke, Planetary Science Institute, 1700 East Ft. Lowell, #106, Tucson, AZ 85719, USA. (mbourke@psi.edu)
J. E. Bullard, Department of Geography, Loughborough University, Loughborough LE11 3TU, UK.